J Mater Sci (2006) 41:6871–6880
DOI 10.1007/s10853-006-0937-3

# Texture evolution during hot-rolling and recrystallization in B2-type FeAl, NiAl and CoTi intermetallic compounds

**Yasuyuki Kaneno · Tetsuo Yamaguchi · Takayuki Takasugi**

Received: 12 August 2005 / Accepted: 16 December 2005 / Published online: 1 October 2006


**Abstract** The texture evolution during the hot-rolling and the recrystallization of B2-type Fe–48Al, Ni–50Al and Co–50Ti (expressed by at.%) intermetallic compounds were investigated. By hot-rolling at 973 K, Fe–48Al showed a microstructure with coarse grains elongated along rolling direction, while Ni–50Al and Co–50Ti showed a deformed microstructure featured by the heavily distorted (elongated) grains and/or the deformation bands. The hot-rolling texture of Fe–48Al was composed of {111}<uvw>, while those of Ni–50Al and Co–50Ti were composed of {111}<110> and {111}<112>, respectively. After annealing, the recrystallized grains were preferentially nucleated at the grain boundaries for Fe–48Al, and in the heavily distorted regions or the deformation bands for Ni–50Al and Co–50Ti. The orientations of the recrystallized grains were similar with those of the deformed matrix, especially for Ni–50Al and Co–50Ti. The recrystallization textures were generally more dispersive than the hot-rolling texture. Based on these results, the texture evolution during the hot rolling and the recrystallization of the B2-type intermetallic compounds were discussed.

Y. Kaneno (✉) · T. Yamaguchi · T. Takasugi
Department of Materials Science, Graduate School of Engineering, Osaka Prefecture University, 1-1 Gakuen-cho, Naka-ku, Sakai, Osaka 599-8531, Japan
e-mail: kaneno@mtr.osakafu-u.ac.jp

## Introduction

FeAl and NiAl with B2 crystal structure have been investigated over many years not only from fundamental but also from practical point of view, because these compounds exhibit good oxidation resistance and reasonable strength at elevated temperatures, and have the benefits of relatively low density and low cost [1, 2]. On the other hand, CoTi with B2 crystal structure shows a high chemical stability and a positive temperature dependence of yield strength [3–5]. Therefore, these intermetallic compounds have been considered to possess a high potential for high-temperature structural and chemical applications.

B2-type intermetallic compounds as well as many other intermetallic compounds are generally brittle at room temperature but they can be plastically deformed at elevated temperatures.Actually, FeAl [6–8], NiAl [9–16] and CoTi [17] have been reported to be hot-worked by conventional extrusion or rolling. Therefore, the microstructural control by thermomechanical processing could be available to these intermetallic compounds. In general, microstructural control relating to grain size, crystallographic texture and grain boundary character are of importance for the development of metallic materials including intermetallic compounds because these factors strongly affect the mechanical properties of materials. Particularly, the knowledge of texture is important for intermetallic compounds, which generally show strong orientation anisotropy in their physical properties.

The textures of the plastically deformed FeAl alloys [18, 19] including (imperfect B2 or $D0_3$) $Fe_3Al$ alloys [20–23] and NiAl alloys [9–16] have been reported. However, there are few studies on rolling

and recrystallization textures of B2-type intermetallic compounds, except for CuZn [24] and NiTi [25]. Recently, the present authors have studied the rolling workability, the texture evolution during the hot rolling at 1273 K and the subsequent annealing behavior of FeAl, NiAl and CoTi [26]. It was shown that FeAl with various contents of Al, and stoichiometric NiAl and CoTi were successfully hot-rolled at 1273 K. Also, the rolling texture reported in (disordered) bcc materials was found to be dominated in these hot-rolled B2 compounds. However, whether the hot-rolling textures observed in the previous study [26] were caused only by the rolling deformation or by the combination of the rolling deformation and the recrystallization was not clarified because the recrystallization more or less occurred during hot rolling at 1273 K. In the present study, Fe–48Al, Ni–50Al and Co–50Ti (at.%) were hot-rolled at 973 K where the recrystallization was suppressed, and then were partially or completely recrystallized. The texture evolution during hot rolling and recrystallization was measured by means of the EBSD (Electron backscattered diffraction) technique together with the X-ray pole figure method. Based on these results, the formation mechanism responsible for the rolling and recrystallization textures of FeAl, NiAl and CoTi was discussed.

## Experimental procedure

Three kinds of Fe–48Al, Ni–50Al and Co–50Ti compounds were used in this study. Purity of each raw material used was 99.9 wt.%. All the compounds were prepared by arc melting in an argon gas atmosphere on a copper hearth using a non-consumable tungsten electrode. Homogenization heat treatment was conducted in a vacuum at 1373 K for 24 h (Fe–48Al), at 1323 K for 48 h (Ni–50Al) and at 1473 K for 48 h (Co–50Ti), respectively, followed by furnace cooling. The homogenized material with a thickness of ~10 mm was sheathed with a stainless steel, and then hot-rolled at 1273 K to ~60% reduction. The rolled sheets were further hot-rolled at 973 K to ~60% reduction. Hot rolling was conducted by a two-roll mill with a roll size of $120^{\phi} \times 180$ mm using an average draught of 0.1 mm. The rolling speed was approximately $1.8 \times 10^{-1}$ m/s. The rolled material was heated every one pass. To obtain partially and completely recrystallized microstructures, the hot-rolled sheets were annealed in various conditions shown in Table 1. Annealing was conducted in a Thermo Riko infrared vacuum furnace (IVF298W) at a heating rate of 100 K/s. The sample was heated up to a desired temperature and held exactly for a desired time, followed by furnace cooling. No vacancy elimination treatment was carried out for all the compounds in this study. For microscopic observation, specimens were first mechanically and then electrolytically polished in a solution of 5% $HClO_4$ and 95% $C_2H_5OH$ at ~278 K. The grain structures were observed by an optical microscope after etching in a solution of 10 ml HCl + 30 ml $HNO_3$ + 60 ml $C_2H_5OH$ for Fe–48Al and 2 ml HF + 4 ml $HNO_3$ + 94 ml $H_2O$ for Ni–50Al and Co–50Ti. The specimens with 1 mm thickness for TEM observation were cut from the hot-rolled sheets using a precision wheel cutting machine. They were mechanically abraded to approximately 0.1 mm thickness and then jet-polished in a solution of 5% $HClO_4$ + 95% $C_2H_5OH$ at 273 K. TEM observation was carried out using a JEOL JEM-2000FX at 200 kV. For microhardness measurement, more than ten data points were collected using mainly a load of 200 g. Macrotexture was evaluated by means of conventional X-ray pole figure method using samples with a size of ~$20 \times 20$ mm$^2$. Two incomplete pole figures, {110} and {200} were measured up to a maximal tilt angle of 75° by the Schultz reflection method [27] and were corrected by using the randomly oriented powder sample. For microtexture, local orientations were determined by the SEM-EBSD using a JEOL JSM-5600 SEM (W filament) equipped with the software (INCA Crystal®) developed by OXFORD INSTRUMENTS®. The corresponding misorientation angles between neighboring grains and grain boundary character distribution (GBCD) were determined from the EBSD data.

**Table 1** Annealing conditions for the recrystallization of the compounds used in this study

| Condition | Fe–48Al | Ni–50Al | Co–50Ti |
|---|---|---|---|
| Partially-recrystallized | 1173 K–10 s | 1023 K–10 s or 1073 K–10 s | 1173 K–10 s or 1223 K–10 s |
| Fully-recrystallized | 1273 K–10 s. | 1273 K–60 s | 1273 K–300 s |

## Results

### Hot-rolled state

All the compounds used in this study were successfully hot-rolled at 973 K as well as at 1273 K [26]. Although an edge cracking somewhat occurred, no significant damage (crack) was observed in any sheets. Initial

grain sizes of the homogenized (i.e., unrolled) specimens were approximately 1 mm for Fe–48Al, 300 μm for Ni–50Al and 150 μm for CoTi, respectively. Figure 1 shows optical micrographs of the hot-rolled compounds. Hot-rolled Fe–48Al shows a microstructure with coarse grains elongated along rolling direction. In contrast, hot-rolled Ni–50Al and Co–50Ti showed a deformed microstructure featured by heavily distorted (elongated) grains. Deformation bands, which have been often observed in deformed microstructure of coarse-grained materials or single crystals [28], are observed for hot-rolled Ni–50Al and Co–50Ti. The difference in the deformed microstructures between Fe–48Al and the others (i.e., Ni–50Al and Co–50Ti) are considered to be primarily due to their initial grain sizes. Figure 2 shows TEM bright field micrographs in the longitudinal section of the hot-rolled compounds. The dislocation structure is considerably different between Fe–48Al and the others (i.e., Ni–50Al and Co–50Ti). For Fe–48Al, the dislocation distribution is homogeneous while for Ni–50Al and Co–50Ti, the dislocation distribution is inhomogeneous. These TEM micrographs suggest that all the hot-rolled specimens do not show the recrystallized microstructure but the deformed microstructure. Microhardness of the as-homogenized (unrolled) and hot-rolled specimens is shown in Fig. 3. The hardness of Fe–48Al is higher than that of Ni–50Al and Co–50Ti. It is known that the thermal vacancies are easily introduced in the FeAl and NiAl intermetallic compounds [29–31]. These thermal vacancies cause a prominent hardening, particularly for FeAl. In general, recovery or recrystallization often occurs during hot-rolling because of high temperature deformation. However, the present observation indicates that during hot rolling at 973 K, recrystallization did not occur so much in Ni–50Al and Co–50Ti.

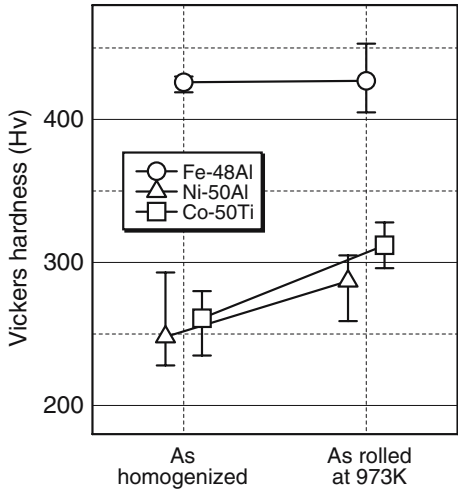


**Fig. 3** Vickers microhardness of Fe–48Al, Ni–50Al and Co–50Ti in the as-homogenized (unrolled) and hot-rolled (at 973 K) states, respectively

Texture analysis was conducted using {100} ({200}) and {110} pole figures and preferred orientations were determined from these two pole figures. Figure 4 shows {100} X-ray pole figures of the hot-rolled compounds. The hot-rolling texture of Fe–48Al consists of orientations with a {111} plane parallel to the sheet surface (i.e., {111}<uvw>). Additionally, {100} textural component, {100}<011>, is recognized in Fe–48Al. On the other hand, {111}<110> and {111}<112> orientations are prominent in the hot-rolling textures of Ni–50Al and Co–50Ti, respectively. Combining with the results of the microscopic observations (Figs. 1, 2) and the hardness measurements (Fig. 3), the hot-rolling textures of the present compounds are assumed

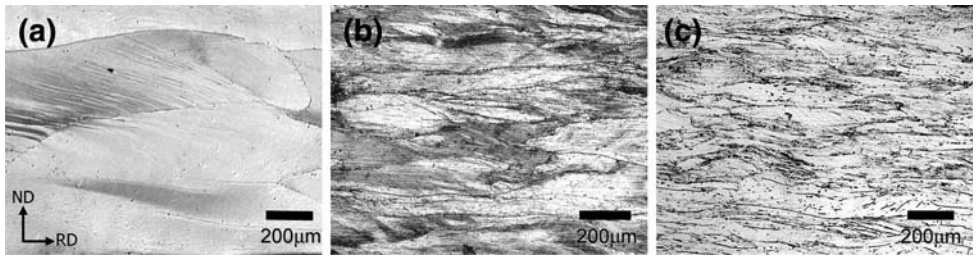


**Fig. 1** Optical micrographs of (**a**) Fe–48Al, (**b**) Ni–50Al and (**c**) Co–50Ti hot-rolled at 973 K. RDand ND indicate rolling and normal directions, respectively

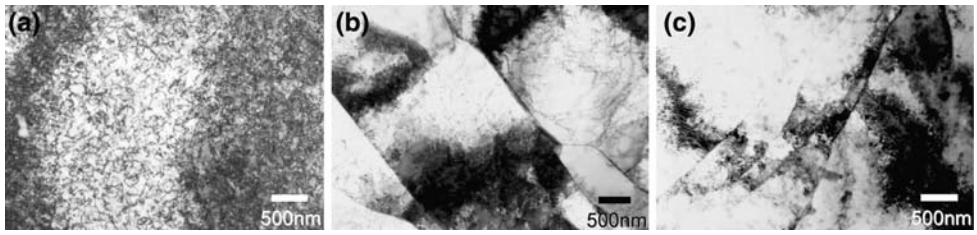


**Fig. 2** TEM bright field micrographs in the longitudinal section of hot-rolled (**a**) Fe–48Al, (**b**) Ni–50Al and (**c**) Co–50Ti. The incident direction of electron beam is [110]

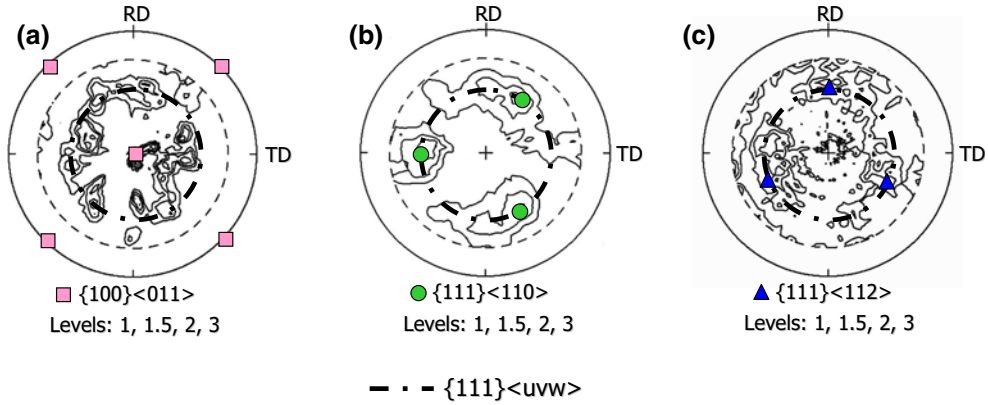


**Fig. 4** {100} pole figures of (**a**) Fe–48Al, (**b**) Ni–50Al and (**c**) Co–50Ti hot-rolled at 973 K. Dashed lines indicate {111}<uvw>

to be developed not by recrystallization but mainly by deformation. Also, the textural components formed by hot-rolling at 973 K are essentially similar to those formed by hot-rolling at 1273 K [26]. In rolling of disordered bcc materials such as iron and low carbon steels, two types of fiber textural components have been developed. One is the $\alpha$-fiber which comprises orientations with a common crystallographic <110> direction parallel to the rolling direction (RD): in the $\alpha$-fiber, {001}<110>, {112}<110> and {111}<110> exist as major components [32]. Another is the $\gamma$-fiber which contains all orientations with a {111} plane parallel to the sheet surface, including {111}<110> and {111}<112> orientations as major components [32]. Basically, the observed hot-rolling textures of the present B2-type compounds are the same as those of many disordered bcc materials.

## Partially-recrystallized state

Figure 5 shows optical micrographs of the partially recrystallized Fe–48Al, Ni–50Al and Co–50Ti. In

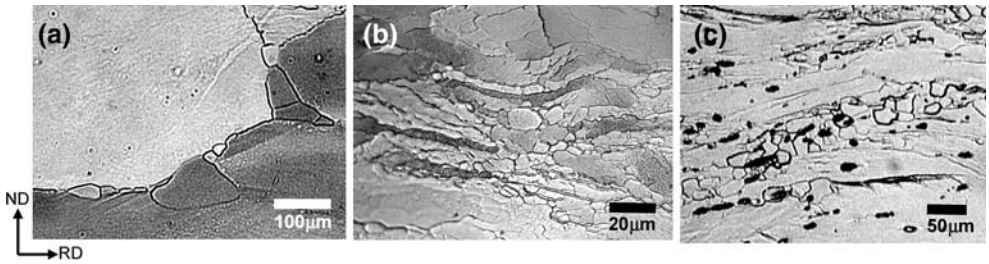


**Fig. 5** Optical micrographs of the partially recrystallized (**a**) Fe–48Al (1173 K–10 s), (**b**) Ni–50Al (1023 K–10 s) and (**c**) Co–50Ti (1173 K–10 s). RD and ND indicate rolling and normal directions, respectively

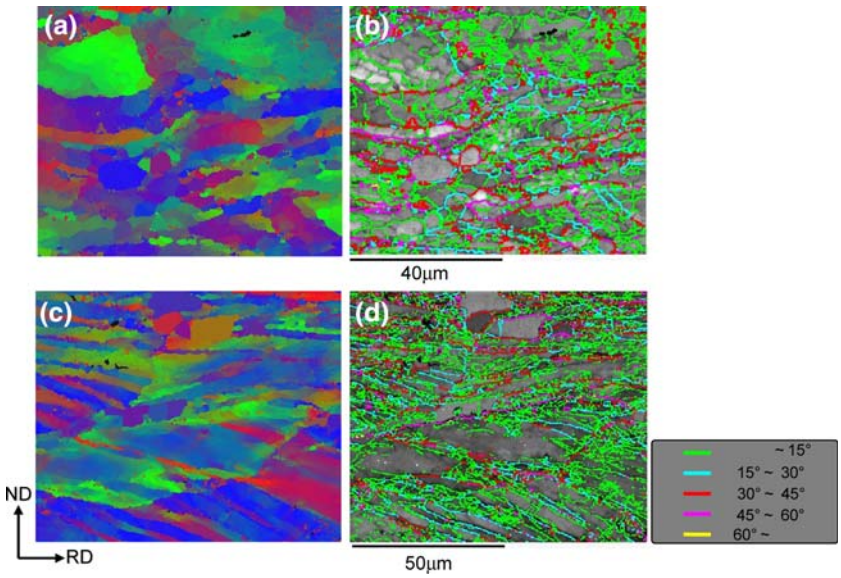


**Fig. 6** The crystal orientation maps (COM) (**a**, **c**) and the boundary maps (**b**, **d**) for the partially recrystallized Ni–50Al (1023 K–10 s) (**a**, **b**) and Co–50Ti (1173 K–10 s) (**c**, **d**) at the normal direction. The color coding for classification of grain boundaries is shown in the figure

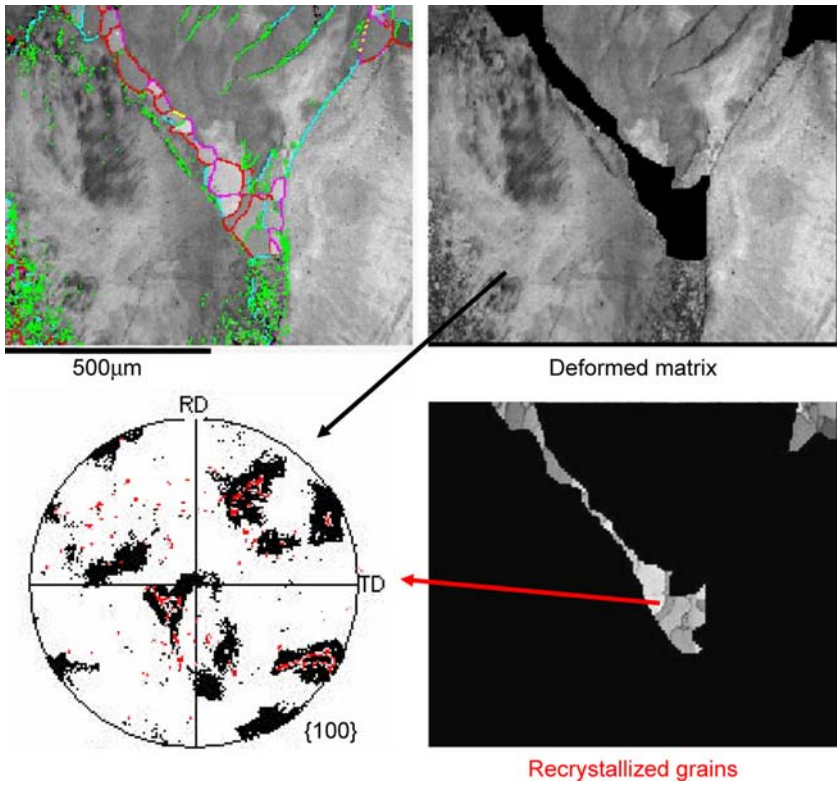


**Fig. 7** The EBSD grain maps, pattern quality images and {100} pole figures for the partially recrystallized Fe–48Al (1173 K–10 s). The color coding for classification of grain boundaries is the same as shown in Fig. 7

Fe–48Al, the recrystallized grains were observed mostly at the grain boundaries. On the contrary, the recrystallized grains in Ni–50Al and Co–50Ti were observed primarily in heavily distorted grains (and/or deformation bands). Thus, the preferential nucleation sites at the early stage of the recrystallization are

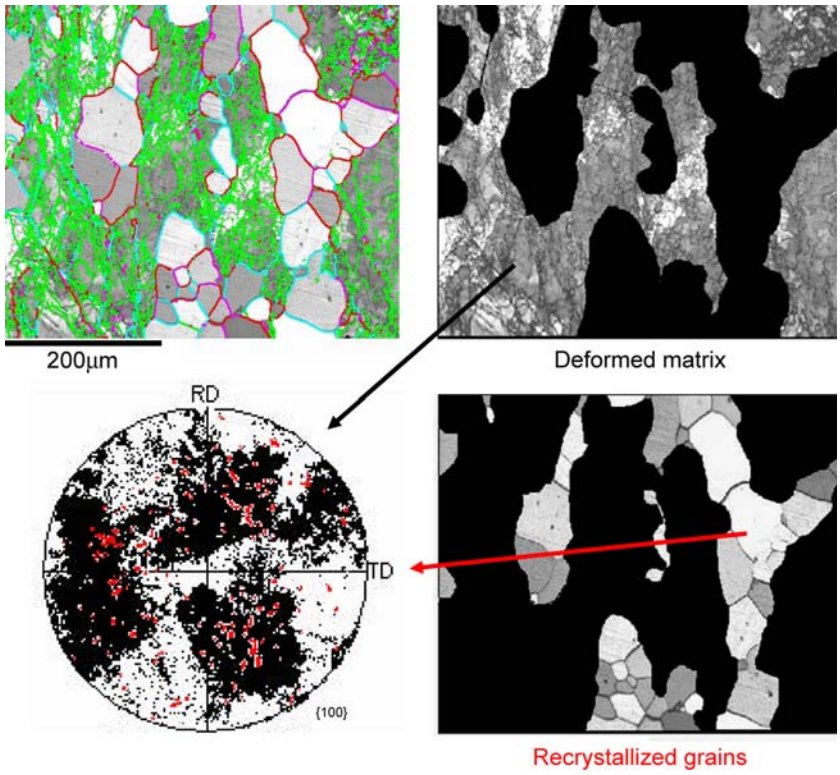


**Fig. 8** The EBSD grain maps, pattern quality images and {100} pole figures for the partially recrystallized Ni–50Al (1073 K–10 s). The color coding for classification of grain boundaries is the same as shown in Fig. 7

different between Fe–48Al and the others (i.e., Ni–50Al and Co–50Ti).

The crystal orientation maps (COM) and the boundary maps for the partially recrystallized Ni–50Al and Co–50Ti at the normal direction are shown in Fig. 6. In the boundary map, low-angle boundaries (LABs) whose misorientation angles are below 15° are colored as green. The banded structures, which are assumed to be recovered deformation bands, are clearly observed. Also, LABs are frequently observed within the deformed (recovered) matrix including the (recovered) deformation bands, suggesting that subgrains are formed in the deformed (recovered) matrix of Ni–50Al and Co–50Ti.

Figures 7–9 show the results of the EBSD analysis for the partially recrystallized Fe–48Al, Ni–50Al and Co–50Ti, respectively. In these figures, the EBSD grain maps, pattern quality images and {100} pole figures are drawn. The color code for grain boundaries in the grain maps is the same as that given in Fig. 6. In the pole figures, the orientations of the grains were separately plotted as deformed (recovered) matrix and recrystallized grains. For Fe–48Al in which the recrystallized grains are preferentially formed at grain boundaries, the grain boundaries are mostly composed of high angle boundaries over 30° which are colored as red or purple in this figure. Consequently, the distribution of the grain boundary misorientation for Fe–48Al shows a peak at ~45° as shown in Fig. 10, and is therefore almost identical to that of a randomly orientated material [33] whose distribution of misorientation angle is included in the figure. The pole figure also indicates that the new grains not only with similar to but also different from orientations of the deformed (recovered) grains are formed. For Ni–50Al (Fig. 8) and Co–50Ti (Fig. 9), a number of low-angle boundaries (LABs) are found in the deformed (recovered) matrix: the observed grain boundaries are mostly composed of misorientation angles between 15° and 30°, which are colored as a light blue in these figures. Consequently, the distributions of misorientation angle for Ni–50Al and Co–50Ti show a peak at misorientation angles of 20°–25°as shown in Fig. 10, and are therefore different from that for Fe–48Al. The EBSD pole figures indicate that the orientations of the recrystallized grains (red points) mostly exist within the orientation distribution of the deformed matrix (black points). From the EBSD results (Figs. 6, 8 and 9), it is suggested that subgrain coalescences partly occur at the early stage of recrystallization in Ni–50Al and Co–50Ti because many subgrains are formed in the recovered matrix and the orientations of recrystallized grains are similar to those of the recovered matrix. However, it is also found from the EBSD pole

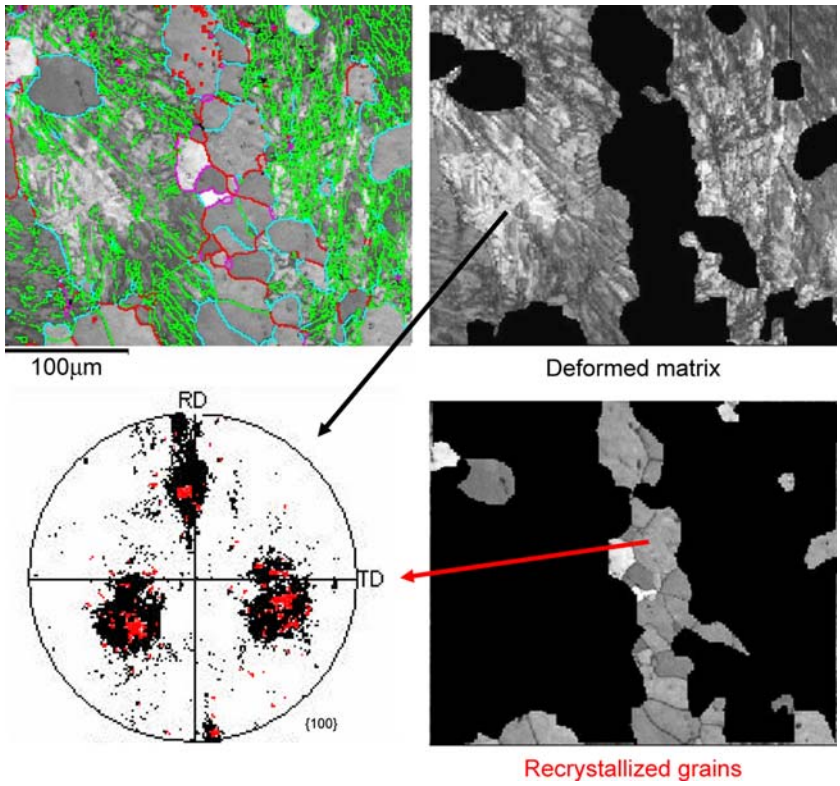


**Fig. 9** The EBSD grain maps, pattern quality images and {100} pole figures for the partially recrystallized Co–50Ti (1223 K–10 s). The color coding for classification of grain boundaries is the same as shown in Fig. 7

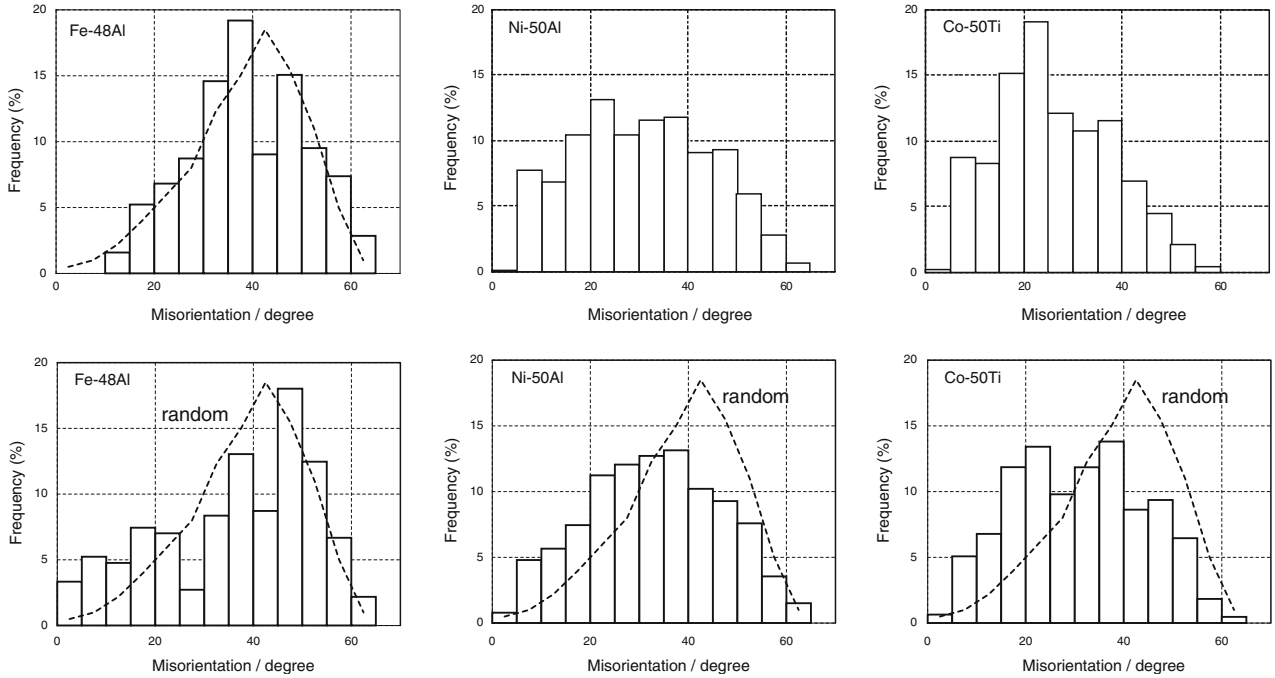


**Fig. 10** The upper row: distribution of the grain boundary misorientation between the recrystallized and deformed (recovered) matrix for the partially recrystallized Fe–48Al (1173 K–10 s), Ni–50Al (1073 K–10 s) and Co–50Ti (1223 K–10 s). The lower row: distribution of the grain boundary misorientation for the fully recrystallized Fe–48Al (1273 K–10 s), Ni–50Al (1273 K–60 s) and Co–50Ti (1273 K–300 s). Broken line shows the distribution of misorientation angle for a randomly oriented material [29]

figures that some recrystallized grains with orientations different from those of the deformed (recovered) matrix are formed.

## Fully recrystallized state

The hot-rolled compounds were fully annealed at 1273 K for 10 s (Fe–50Al), 60 s (Ni–50Al) and 300 s (Co–50Ti), respectively. The optical micrographs of the fully recrystallized compounds are shown in Fig. 11. All the compounds consist of equiaxed grains. The average grain sizes of the fully recrystallized specimens are 178 μm for Fe–48Al, 62 μm for Ni–50Al and 37 μm for Co–50Ti, respectively. The observed large grain size for Fe–48Al may be due to the large initial grain size of the unrolled specimen.

Figure 12 shows {100} pole figures of the fully recrystallized compounds, whose microstructures are given in Fig. 11. The recrystallization textures consist of considerably scattered (random) orientations compared with the hot-rolling texture, though the preferred orientations in the hot-rolling texture still retained after the complete recrystallization.

The distributions of grain boundary misorientation angle for the fully recrystallized compounds are shown in Fig. 10. Again, the distribution of misorientation angle for a randomly oriented material [33] is included in this figure. For Fe–48Al, the distribution of misorientation angle for the fully recrystallized specimen is similar to that for the partially recrystallized specimen and basically analogous to that for a randomly oriented material [33]. For Ni–50Al and Co–50Ti, the peak at

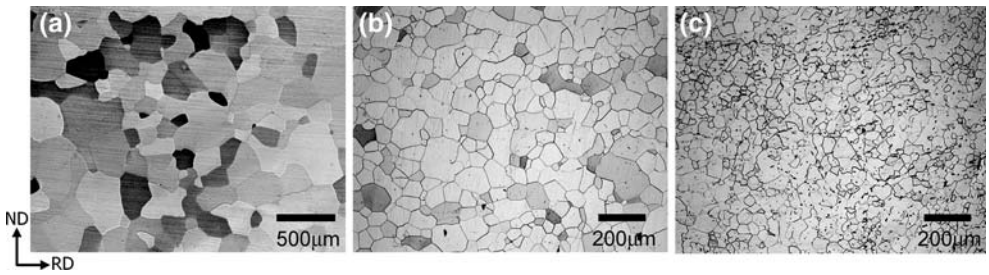


**Fig. 11** Optical micrographs of the fully recrystallized (**a**) Fe–48Al (1273 K–10 s), (**b**) Ni–50Al (1273 K–60 s) and (**c**) Co–50Ti (1273 K–300 s). RD and ND indicate rolling and normal directions, respectively

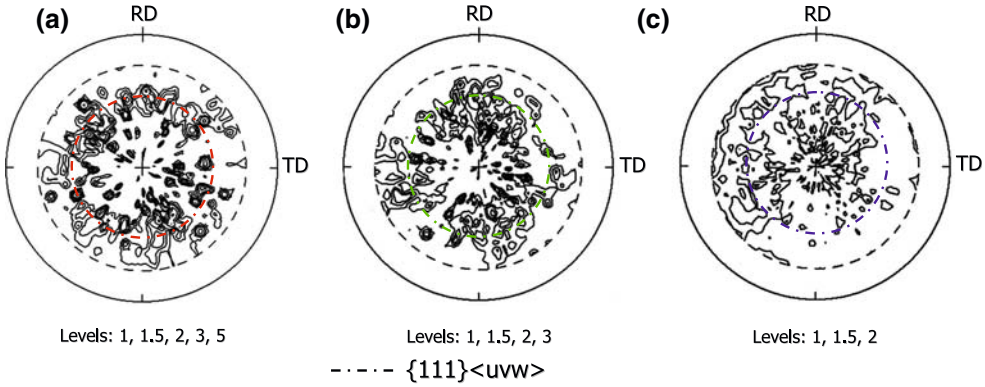


**Fig. 12** {100} pole figures of the fully recrystallized (**a**) Fe–48Al (1273 K–10 s), (**b**) Ni–50Al (1273 K–60 s) and (**c**) Co–50Ti (1273 K–300 s). Solid broken lines indicate {111}<uvw>

misorientation angles of 20°–25° shifts toward a higher angle by complete recrystallization and therefore changes to that for a randomly orientated material. These results correspond to the macrotexture measured by X-ray diffraction (Fig. 12).

The grain boundary character distribution (GBCD) for the fully recrystallized specimens is shown in Fig. 13. In this figure, the Brandon criterion: $\Delta\theta_{max} = 15°\Sigma^{-1/2}$ was used to classify the grain boundary character in terms of the coincidence site lattice (CSL) model [34]. The GBCDs are primarily characterized by a high frequency (~10–15%) of Σ1 boundaries, i.e., low-angle boundaries (LABs) besides random (i.e., 29 < Σ) boundaries. No significant occurrence of other special (i.e., 3 ≤ Σ ≤ 29) boundaries is found in all the compounds.

## Discussion

### Hot-rolling texture

Deformation texture is formed by a crystal lattice rotation due to slip deformation, and therefore closely associated with the activated slip systems. As the slip system of FeAl, NiAl and CoTi activated at elevated temperatures, it is well known that <100>{011} commonly operates [35–38]. As the minor slip systems activated at elevated temperatures, <111>{011} for FeAl [35, 36], and <100>{001} and <110>{001} for NiAl and CoTi [38–41] have been reported. Therefore, the deformation texture of FeAl, NiAl and CoTi developed at high temperatures should be similar one another because the same slip system of <100>{011} operates in these B2 compounds. Consequently, the observed hot-rolling textures are in common composed of a <111>//ND textural component (i.e., {111}<uvw>) (Fig. 4).

Some studies have reported that a <110>-fiber texture is formed in hot-extruded NiAl [10–14], while a <111> fiber texture is formed in compressed NiAl [14–16] and FeAl [19]. On the other hand, the texture developed during tension and compression of polycrystalline NiAl has been simulated, assuming that <100>{011} and <100>{001} slip systems are operating [16]. According to this simulation, <100>{001} slip system does not contribute to the textural development, and alternatively, <100>{011} slip system dose contribute to <110> and <111> fiber textures developed in tension and compression modes, respectively. The stress system in rolling deformation is assumed to be composed of the compressive stress normal to the rolling plane and the tensile stress parallel to the rolling direction [42]. Therefore, the texture consisting of {111} parallel to the rolling plane and <110> parallel to the rolling direction, that is, {111}<110> orientation is expected to be developed in polycrystalline NiAl by rolling deformation. In fact, this orientation was observed in hot-rolled Ni–50Al (Fig. 4). Thus, a slip system of <100>{011} is suggested to play an important

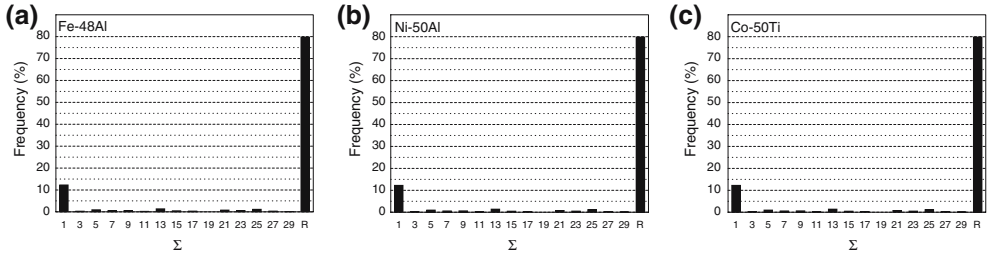


**Fig. 13** Distribution of the grain boundary character for the fully recrystallized (**a**) Fe–48Al (1273 K–10 s), (**b**) Ni–50Al (1273 K–60 s) and (**c**) Co–50Ti (1273 K–600 s)

role on the formation of the rolling texture for the present B2-type intermetallic compounds. However, if only the <100> dislocations are activated by high temperature deformation, sufficient independent slip systems are not provided, that is, the von Mises' criterion is not satisfied. Therefore, it is likely that the diffusion-assisted restorative processes such as recovery (and recrystallization) also occur during hot rolling [43].

A minor difference in the hot-rolling texture among the present compounds is that a {100} textural component, {100}<011> (i.e., α-fiber component) is present in the hot-rolled Fe–48Al, but not in the hot rolled Ni–50Al and Co–50Ti. For the cold-rolling texture of FeCo that undergoes an order (B2)-disorder (bcc) transition [44], it has been reported that the intensity of α-fiber component is lower than those of γ-fiber component when alloy is ordered state. The ordering energy of FeAl is lower than that of NiAl and CoTi, as simply estimated from their melting points. In other words, FeAl is considered to be a weakly ordered alloy, consequently resulting in favorable formation of the α-fiber component in the hot-rolling texture of Fe–48Al. However, the premature occurrence of the recrystallization during the hot-rolling, and the influence of initial grain size and starting texture formed during solidification cannot be excluded from possible factors affecting the observed rolling texture.

### Recrystallization texture

The nucleation sites of the recrystallized grains in Ni–50Al and Co–50Ti are obviously different from those in Fe–48Al. In the case of Fe–48Al with a coarse grain size, deformation behavior is inhomogeneous and large stress concentration takes place at the vicinity of grain boundaries. Consequently, new grains are preferentially formed at grain boundaries. In the case of Ni–50Al and Co–50Ti, the recrystallized grains were preferentially formed in the heavily distorted grains and/or the deformation bands (Figs. 5, 6, 8 and 9). The EBSD boundary maps (Fig. 6) reveal that many subgrains surrounded by subboundaries (LABs) are formed within the deformed grains and the deformation bands. It is therefore suggested that subgrain coalescences partly takes place at the earl stage of recrystallization (i.e., partially recrystallized state), resulting in formation of recrystallized grains with similar orientations to the deformed (recovered) matrix. However, at the same time, some recrystallized grains with orientation dissimilar to the deformed (recovered) matrix are recognized in the EBSD pole figures. Also, it was found that there is no specific orientation relationship (misorientation angle) between the recrystallized grains and the deformed grains. Moreover, the subsequent grain growth proceeds in the absence of formation of preferred orientations, suggesting the *non-selected grain growth*. Consequently, the recrystallization texture more or less becomes random though the preferred orientations developed in the hot rolling still remained even after the complete recrystallization.

The observed recrystallization texture becomes more random (dispersive) with proceeding recrystallization, especially for Ni–50Al and Co–50Ti. Recent modeling for the recrystallization textures by Sebald and Gottstein reveals that the texture is fairly changed and at the same time, intensified by recrystallization if grain boundaries with a specific misorientation have a high mobility, but the texture is weakened by recrystallization if there are no specific grain boundaries with a high mobility [45]. In highly ordered B2 and $L1_2$ alloys, it is assumed that when a grain boundary moves, disordering occurs, and simultaneously, reordering is required. This phenomenon includes the effect of retarding the grain growth [15], and also does not result in significant anisotropy in the grain growth stage between specific and non-specific grain boundaries, particularly at high temperature [46]. In fact, weakly formed recrystallization texture has been repeatedly observed in cold rolled $L1_2$-type ordered alloys such as $Ni_3Al$ [47, 48], $Ni_3$ (Si, Ti) [49] and $Co_3Ti$ [50].

## Conclusion

B2-type Fe–48Al, Ni–50Al and Co–50Ti (expressed by at.%) intermetallic compounds were hot-rolled and subsequently annealed. The texture development during hot-rolling and recrystallization was investigated by means of X-ray pole figure and the EBSD. The following results were obtained:

1. All the compounds used in this study were successfully hot-rolled at 973 K, leading to the formation of the deformed microstructure, particularly for Ni–50Al and Co–50Ti.
2. The hot-rolling textures of Fe–48Al, Ni–50Al and Co–50Ti are commonly composed of a ND//{111} textural component although the orientation distribution and its intensity were somewhat different among three compounds.
3. The preferential nucleation sites of new grains at the early stage of the recrystallization were the grain boundaries for Fe–48Al, and the heavily distorted grains and/or the deformation bands for Ni–50Al and Co–50Ti.

4. The orientations of the recrystallized gains were evolved within the orientation distribution of the deformed matrix, but were more dispersive than those of the deformed grains. It was suggested that the non-selected grain growth was responsible for the observed weak recrystallization textures of the present compounds.

**Acknowledgements** This work was supported in part by the Grant-in-aid for Scientific Research from the Ministry of Education, Culture, Sports and Technology, Japan.

## References

1. Noebe RD, Bowman RR, Nathal MV (1996) In: Stoloff NS, Sikka VK (eds) Physical metallurgy and processing of intermetallic compounds. Chapman & Hall, New York, pp 212–296
2. MaKamey CG (1996) In: Stoloff NS, Sikka VK (eds) Physical metallurgy and processing of intermetallic compounds. Chapman & Hall, New York, pp 351–391
3. Takasugi T, Izumi O (1987) Phys Stat Sol (a) 102:697
4. Takasugi T, Izumi O (1988) J Mater Sci 23:1265
5. Kaneno Y, Takasugi T (2003) J Mater Sci 38:869
6. Pang L, Han SM, Kumar KS (2002) Acta Mater 50:3623
7. Lin D, Li D, Li Y Intermetallics 6(199):243
8. Alexandeer DJ, Maziasz PJ, Wright JL (1998) Mater Sci Eng A258:276
9. Harris KE, Ebrahimi F, Garmestani H (1998) Mater Sci Eng A247:187
10. Khadkikar PS, Michal GM, Vedula K (1990) Metall Trans 21A:279
11. Dymek S, Hwang SJ, Dollar M Kallend JS, Nash P (1992) Scripta Metall Mater 27:161
12. Margevicius RW, Lewandowski JJ (1993) Scripta Metall Mater 29:1651
13. Margevicius RW, Cotton JD (1995) Acta Metall Mater 43:645
14. Zhao XB (1998) J Mater Sci Lett 17:489
15. Fischer-Buhner J, Raabe D, Wagner P, Gottstein G (1995) Scripta Metall Mater 33:1261
16. Ahzi S (1999) Mater Sci Eng 7:841
17. Kaneno Y, Takasugi T, Hanada S (2001) Mater Sci Eng A302:215
18. Morris DG, Deevi SC (2002) Mater Sci Eng A329–331:573
19. Sakata T, Kohma H, Yasuda H, Umakoshi Y (2002) ISIJ Int 42:903
20. Rabbe D, Mao W (1995) Phil Mag A71:805
21. Rabbe D, Keichel J, Sun Z (1996) J Mater Sci 31:339
22. Kad BK, Schoenfeld SE, Asaro RJ, Mckamey CG, Sikka VK (1997) Acta Mater 45:1333
23. Huang YD, Yang WY, Chen GJ, Sun ZQ (2001) Intermetallics 9:331
24. Zhu GH, Mao W, Yu Y, Brückner G (1999) Proc Int Conf Textures Mater (ICOTOM-12) Ed. by Szpunar JA NRC Research Press, Ottawa, 629–634
25. Inoue H, Miwa N, Inakazu N (1996) Acta Mater 44:4825
26. Kaneno Y, Yamaguchi T, Takasugi T (2005) J Mater Sci 40:733
27. Schultz LG (1949) J Appl Phys 29:1030
28. Inokuchi Y, Doherty RD (1978) Acta Metall 26:61
29. Nagpal P, Baker I (1991) Metall Trans 21A:2281
30. Morris MA, George EP, Morris DG (1998) Mater Sci Eng A258:99
31. Xiao H, Baker I (1995) Acta Metal Mater 43:391
32. Humphreys FJ, Hatherly M (1995) Recrystallization and related annealing phenomena. Elsevier Science, Oxford
33. Mackenzie JK (1964) Acta Metall 12:223
34. Brandon DG (1966) Acta Metall 12:1479
35. Umakoshi Y, Yamaguchi M (1980) Phil Mag A41:573
36. Umakoshi Y, Yamaguchi M (1981) Phil Mag A44:711
37. Noebe RD, Bowman RR, Nathal MV (1993) Inter Mater Rev 38:193
38. Takasugi T, Tsurisaki K, Izumi O, Ono S (1990) Phil Mag A61:785
39. Kim JT, Gibala R (1991) Mater Res Soc Symp Proc 213:261
40. Field RD, Lahrman DF, Darolia R (1991) Acta Metal Mater 39:2951
41. Takasugi T, Yoshida M, Kawabata T (1992) Phil Mag A65:29
42. Dillamore IL, Roberts WT (1964) Acta Metall 12:281
43. Baker I, Schulson EM (1984) Metal Trans A 15A:1129
44. Zhu G, Mao W, Yu Y (1999) Prog Nat Sci 9:849
45. Sebald R, Gottstein G (2002) Acta Mater 50:1587
46. Aust KT, Rutter JW (1962) Trans AIME 224:111
47. Gottstein G, Nagpal P, Kim W (1989) Mater Sci Eng A108:165
48. Escher C, Neves S, Gottstein G (1998) Acta Mater 46:441
49. Kaneno Y, Nakaaki I, Takasugi T (2002) Intermetallics 10:693
50. Kaneno Y, Nakaaki I, Takasugi T (2002) J Mater Res 17:2567